ADVANCES IN MATERIALS SCIENCE, Vol. 20, No. 3(65), September 2020

sciendo

DOI: 10.2478/adms-2020-0016

A. Tamadon*, M. Abdali, D. J. Pons, D. Clucas

University of Canterbury, Department of Mechanical Engineering, Christchurch 8041, New Zealand

**abbas.tamadon@pg.canterbury.ac.nz*

CHARACTERIZATION OF DISSIMILAR Al-Cu BFSW WELDS; INTERFACIAL MICROSTRUCTURE, FLOW MECHANISM AND INTERMETALLICS FORMATION

ABSTRACT

The purpose of this study is to elucidate the flow features of the dissimilar Al-Cu welded plates. The welding method used is Bobbin Friction Stir Welding (BFSW), and the joint is between two dissimilar materials, aluminium alloy (AA6082-T6) and pure copper. Weld samples were cut from along the weld line, and the cross-sections were polished and observed under an optical microscope (OM). Particular regions of interest were examined under a scanning electron microscope (SEM) and analysed with Energy Dispersive X-ray Spectroscopy (EDS) using the AZtec software from Oxford Instruments. The results and images attained were compared to other similar studies. The reason for fracture was mainly attributed to the welding parameters used; a higher rotational speed may be required to achieve a successful BFSW between these two materials. The impact of welding parameters on the Al-Cu flow bonding and evolution of the intermetallic compounds were identified by studying the interfacial microstructure at the location of the tool action. The work makes an original contribution to identifying the solid-phase hybrid bonding in Al-Cu joints to improve the understanding of the flow behaviours during the BFSW welding process. The microstructural evolution of the dissimilar weld has made it possible to develop a physical model proposed for the flow failure mechanism.

Keywords: Bobbin Friction Stir Welding; AA6082-T6; copper; intermetallics; weld defects

INTRODUCTION

Aluminium to copper dissimilar welds are a highly applicable hybrid joint, necessary for high-tech industrial applications, where it is needed to meet specific ductility or low-weight requirements, as well as providing thermal and/or electrical conductivity, with corrosion resistance [1]. Examples of high-performance Al-Cu welds used include electronic industries, transportation vehicles, energy industries, and aerospace components [2].

Regarding the Al-Cu weld quality, there is a challenge in conventional joining techniques for these two incompatible materials, due to their distinct physical and chemical

characteristics. In general, fusion welding is not a recommended process as a large number of Inter-Metallic Compounds (IMCs) are formed during this welding process, and a sound weld is difficult to achieve a defect-free structure [1].

Since the thermomechanical mechanism of the joining process in friction stir welding (FSW) occurs in solid-state phase, therefore this technique prevents the metallurgical defects related to the solidification occurring in fusion welding. This is because of specific interaction between the non-consumable tool and the substrate in which result in plasticizing and intermixing between dissimilar Al and Cu mass, instead of a fusion welding at the interface.

Despite some success for conventional-FSW weld, the literature reports no evidence of the Bobbin-FSW results for the dissimilar Al-Cu welds. It seems that the bobbin friction stir welding (BFSW) as a young technique still has some difficulties in producing a defect-free Al-Cu weld.

This paper presents a detailed metallurgical experimentation of Aluminium-Copper BFSW weld to evaluate the defect formation mechanism in failed joints. Based on identifying the internal flow characteristics, intermetallic compounds (IMCs) and the Grain-Boundary Engineering (GBE) established by the process, we suggest possible future research approaches for improved weld quality.

As the BFSW is a young welding technique and establishment of an Al-Cu dissimilar joint is inherently difficult regarding the metallurgy of the structure, the examining of the failed welds is worth to reveal the applied factor in the formation of weld defects. Understanding the flow failure mechanism, also the metallurgical transformations in uncontrolled emergence of IMCs can to a large extent identify the origins of the weld defect which directly affect the quality of this dissimilar joint.

IMC’s in fusion welding are uncontrolled metallurgical defects emerging during the solidification, which deteriorate the expected welding properties by lowering strength and increasing brittleness, and electric resistance [3]. In such instances, to avoid the solidification problems, other types of welding methods without a liquid phase, including Friction Stir Welding (FSW), are more suitable for dissimilar joints [4]. FSW is a solid-phase welding method, where processing temperatures are below the melting point of the workpieces [5]. Moreover, no filler metal is used, therefore, the weld region is free of solidification cracking or porosity [6,7]. Besides that, no gases or fumes are produced during the FSW operation compared to fusion welding. Since the working temperature is well below the melting temperature, FSW can provide better control of the formation of IMCs [8]. Also, because of the automation of the operation, the welding parameters can be applied with a high accuracy [9].

FSW was introduced by The Welding Institute (TWI) in 1991 [7], for solid-state welding plates of same or dissimilar materials [6]. By rotating a non-consumable tool between the joint interface and driving along the weld direction, friction heat generation and sufficient shearing force induced by the rotating tool, result in plasticizing and mixing the mass at the interface of the tool-substrate [10]. The frictional interaction at the surface contact between the tool and the workpiece (as the substrate), causes the heat input with -no external heat source- which provides the plasticity of the materials [11], required for the mass flow within the stirring zone (SZ) [12,13].

Bobbin Friction Stir Welding (BFSW) covered in this study uses a bobbin tool; this offers better stability during the welding process [14,15]. The main issue to obtain a sound weld by the BFSW technique is a sound connection between the AA6082- aluminium alloy and Copper (Cu) without any discontinuity through the weld-seam.

LITERATURE REVIEW

Bobbin Friction Stir Welding

Bobbin tools were developed to improve aspects of conventional FSW [16]. The tool consists of two symmetrical shoulders on the workpiece surfaces, connected by a centred pin driven into the butt-joint-line interface [17]. A conventional FSW (CFSW) tool consists of one shoulder and the penetrating probe, requiring a backing anvil bar for support on the opposite plate surface. This can act as a heat sink and has the potential to generate defects in the weld root [18].

A double-sided tool (bobbin tool) overcomes these issues as the tool itself supports the joint, and the root region is removed by a rotating bottom shoulder participating in heat generation and conservation. [19]. BFSW will also provide an even heat input across the weld resulting in less distortion, can accommodate thickness variation, would have low axial forces on the fixture and machine, and provides ease of control due to the force exerted by the shoulders [20,21].

When the tool is rotating and traversing through the joint-line, the pin pinches material from both sides and forges them together in the SZ [13,22,23]. The material is plasticised, and subsequently by the advancing of the tool, forms the weld-seam by repeated deposition of the stirred layers, transported to the trailing edge of the tool [24,25]. By the action of two rotating shoulders, BFSW provides sufficient heat for plastic flow between the Al and Cu faces; being more effective than conventional FSW [10,26].

1.2.2. Dissimilar joints: soft materials

Many methods are used to join two different materials; these could be categorised as per their joint formation mechanism, which can be mechanical, a chemical reaction, an application of thermal energy, or a combination (hybrid process). FSW is a combination of thermal and mechanical joining, where the frictional heat generated by the mechanical performance of the rotating tool softens the material, and the further stirring action mixes and bonds the material.

FSW achieves the solid-state joining of two dissimilar materials at a working temperature much below the melting points (1/3 T_m), even though when the melting temperatures are remarkably different (660°C vs 1085°C, for Al and Cu, respectively) [27,28]. The structure of the FSW joints comprises four typical subdivisions. The main weld region is the stirring zone (SZ), situated at the weld centre and is directly formed by the tool action [29,30]. As the heat generation and the deposition of the plastic mass occurs in the SZ, this region experiences full dynamic recrystallization (DRX) as it cools after the welding process [11,12].

The thermo-mechanically affected zone (TMAZ) at the proximity of the SZ, is the interface between the stirred mass and the unstirred base-metal region of the workpiece. The TMAZ is where the material microstructure is affected by shear strain induced by the mechanical performance of the tool, as well as the thermal flux absorbed from the friction effect [4]. The heat-affected zone (HAZ) is the next region between the TMAZ and the base metal (BM) [31]. HAZ is a common characteristic of all thermal welded joints, influenced by the heat input, affecting the microstructure and mechanical properties. Both the HAZ and TMAZ are known as the transition region in the FSW weld structure, situated between the SZ and the BM [32].

It should be noted that a defect-free interface in dissimilar joints is difficult to achieve due to the narrow weldability window in working temperature. Adjusting the process parameters to achieve an optimized flow, as well as the high chemical interaction between the base metals is required to obtain a successful hybrid joint [33].

Dissimilar joints: partnerships with copper

In many works studying the dissimilar FSW processing of aluminium-copper alloys, joint efficiency of the weld was noted to be less than 100%. The weld microstructure can be divided into two areas: under the shoulder where the SZ and TMAZ are, and outside the shoulder where the HAZ is situated next to the parent material [34].

According to the theory of the FSW process, in an Al-Cu joint, by considering of the clockwise rotation of the tool, it suggests to consider the copper plate at the advancing side (AS), and the aluminium plate at the retreating side (RS) of the weld. This configuration provides better tool performance in interaction with the workpieces, as the tool first softens the workpiece with higher density (Cu) at the AS, and then transport the plasticized mass towards the lower density material (Al at the RS of the weld). As in a clockwise tool rotation, both the heat input and the mass transportation has a AS-to-RS flow direction, the TMAZ shows a wider breadth on the RS (Al-side) than in the AS (Cu-side). This is noted to be due to the tool offset through the weld cross-section, creating more mass circulation, steering toward the Al-side (retreating side), while the lower peak of temperature at the Cu-side (advancing side) will not affect the Cu grains [35]. Similarly, the width of the HAZ usually is larger on the Al-side. This is caused by intense heat but with no grain deformation and would have less hardened coarse grains [36-39].

The microstructure in the SZ of dissimilar FSW shows a intercalated vortex pattern of the lamellae flow lines as the stir-induced shear bands [40]. The stirring action creates swirl-like patterns at the bottom of the weld, while at the upper part of the nugget zone, a composite-like structure is formed. This can be similar to the onion ring structure as typical of the material flow patterns found in the SZ of the FSW joints [41].

The formation of Intermetallic compounds (IMCs) in Al-Cu welds is a major issue, as IMCs are hard and brittle, and would decrease the quality of the weld by creating irregular and fragmented defects. It is normal to find continuous thin layers of IMCs at the Al-Cu interface that would result in a complete joint free from defects, but the brittleness of the IMCs would still make this the weakest zone. Moreover, micro-hardness of the weld nugget is also affected by the IMCs. Commonly found IMCs in Al-Cu FSW joints are $CuAl_2$, Cu_9Al_4, Cu_3Al and CuAl, Al_2Cu and γ_1-Al_4Cu_9 phases were found to be formed in an Al 6082-T6/ Cu FSW [42].

Regardless the metallurgy of the weld, in FSW process, the weld configuration and the welding operational parameters play a major role in creating a high strength joint placing the copper plate on the retreating side in a butt-joint during conventional FSW has been shown to cause macro-size voids or the open tunnel void, while placing Cu on the advancing side would allow for a defect-free weld. A tunnelling defect appears as a continuous pattern of voids beneath the shoulder and above the root of the weld in FSW [43].

High transverse welding speed and low tool rotational speed causes voids and tunnelling defects, due to the insufficient heat input and material flow required for a steadily mass transportation during the stirring action. Very low rotational speeds could also cause pores, which are large voids about 0.1-0.5 mm in diameter [44,45].

On the other hand, extreme process temperatures would create high copper diffusion in the aluminium matrix, leading to more and larger IMCs formation, hence an increase in hardness, more cracks, and lower ultimate tensile strength (UTS) [1]. Macro- and microcracks could also be caused by poor metallurgic bonding between the large copper particles in an aluminium matrix, forming a large discontinuity through the joint-line [46].

Al-Cu Hybrid Joints

Early efforts in Al-Cu FSW were focused on conventional-FSW for lap-joints or spot-welds; the published literature shows insufficient information regarding Al-Cu butt-joint welds by BFSW. In this regard, we aim to identify the mass flow deposition within the hybrid weld region, as well as to characterize the formation of possible intermetallic compounds through the weld structure.

Literature shows that the main challenge to obtain a safe weld in FSW dissimilar joint is the flow instability at the intermixing interface of the Al-Cu substrates. In addition to an optimized flow, the control of the high chemical interaction between Al-Cu base metals is another consideration required to obtain a successful hybrid joint. This can be problematic during the Al-Cu dissimilar welding process, where the uncontrolled formation of the IMCs deteriorates the microstructural and mechanical properties of the joint.

While the BFSW technique is well-established for the processing of aluminium grades, it is problematic for the higher active materials, e.g. dissimilar welds. The Al-Cu hybrid joint in this study is an attractive candidate for evaluation of the weld quality. Hence in order to better understand the challenges with BFSW of Al-Cu joining mechanism, it is necessary to examine the weld microstructure, which has not previously been demonstrated for this hybrid weld.

This paper studies a butt-weld joint between AA6082-T6 and commercially pure (CP) copper plates using the BFSW method, by applying a fixed-gap bobbin-tool. The Al-Cu hybrid weld structure is a subject of microscopic characterization, focusing on the material flow evolution in the SZ area. The impact of welding parameters on the Al-Cu flow bonding and evolution of the intermetallic compounds were identified by the interfacial microstructure at the position of the tool performance. The microscopic flow characterization can help to present a physical model for the elucidation of the material flow interaction at the proximity of the rotating tool in interaction with the mixing mass from Al-side and Cu-side of the weld.

EXPERIMENTAL

Purpose

While BFSW is well-established for softer grades of aluminium, it is problematic for the higher strength grades. Weld quality is difficult to consistently obtain using BFSW for this material. It is becoming apparent that the challenges with BFSW of AA6082-T6 relate to lack of control over the Grain-Boundary Engineering (GBE). And other metallurgy-induced microscopic features (IMCs and GBE)

This study aimed to evaluate the internal flow mechanism observed in the Al-Cu weld structure and analyse the microscopic features within the Stirring Zone (SZ). By comparing the internal microflow patterns between the cross-sections, the origins of the failure will be identified.

The novelty of the methodology is the application of the microstructural observation in the specific case of Al-Cu BFSW processing. By characterization of the origins of the flow failure and the IMCs formation for defective welds, the quality issues can be compared between defective and successful welds of dissimilar materials.

The main limitation was that a successful weld is not available for comparison. Ideally, multiple welds might be performed to provide the means to compare flow regimes. In this regard, the welding speeds (rotational and feed rate) can also be modified to induce a higher rate of plasticising through the stirred mass. Furthermore, the tool geometry also can be

modified to provide more efficient material transportation flow between the AS and RS during the rotation and mass-circulation around the pin.

Materials

The BFSW process was conducted between the two dissimilar materials: CP copper, and a 6xxx series marine-grade aluminium alloy (AA6082-T6). The AA6082-T6 aluminium alloy was used as it is one of the strongest structural Al grades with excellent corrosion resistance. Therefore, compared to other aluminium alloys, regarding the hybrid processing with copper, AA6082-T6 has the most capability for the mechanical interaction with the tool, also a stabilized structure suitable for dissimilar welding. Analysed chemical composition of the aluminium alloy is shown in Table 1 with the elemental details.

Table 1. *Chemical composition of AA6082-T6*

Aluminium Alloy 6082	
Chemical Element	% Present
Silicon (Si)	(0.70–1.30)
Magnesium (Mg)	(0.60–1.20)
Manganese (Mn)	(0.40–1.00)
Iron (Fe)	(0.0–0.50)
Chromium (Cr)	(0.0–0.25)
Zinc (Zn)	(0.0–0.20)
Titanium (Ti)	(0.0–0.10)
Copper (Cu)	(0.0–0.10)
Other (Each)	(0.0–0.05)
Other (total)	(0.0–0.15)
Aluminium (Al)	Balance

Welding

The applied welding parameters for conducted trial tests are shown in Table 2.

The welding process was done by a single piece bobbin tool that consists of a top-shoulder, a bottom-shoulder and a fixed pin in the middle, trajectories.

The bobbin-tool used was a fully-featured tri-flat pin with spiral scrolls on the shoulders (Figure 1). These geometric patterns at the surface of the tool components (centred pin and top and bottom shoulders) can provide sufficient uniformity for the frictional stirring condition between the rotating tool in contact with the workpiece material. The tool was fabricated form H13 tool-steel (560 HV hardness), to assure enough rigidity during the plastic deformation.

Table 2. *Parameters of the BFSW trial for the AA6082-T6/Cu plates*

Welding Parameters	**amount**
$D_{Shoulder}$ (mm)	21
D_{Pin} (mm)	7
$D_{Shoulder}/D_{Pin}$	3:1
Plates Thickness (mm)	6
Compression Ratio	3.75%
Spindle Rotational Speed, ω (rpm)	800
Feed Rate, V (mm/min)	400
Pin Thread Pitch (mm)	1.5
Number of Pin Threads	4

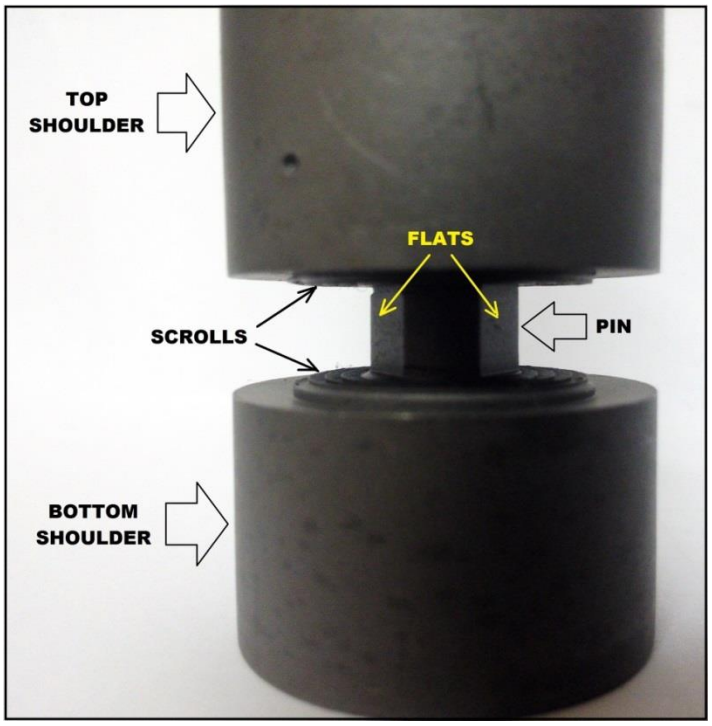

Fig. 1. The bobbin-tool used for the Al-Cu welding trial

The sample preparation procedure followed the method of previous work [4]**.** The BFSW welding trial was conducted by a 3-axis CNC machine (2000 Richmond VMC Model, 600 Group brand, Sydney, Australia) while the bobbin-tool was installed on a spindle motor (Fanuc control unit) with 14-horsepower capacity. The AA6082-T6 aluminium and CP copper plates were arranged in the butt-joint position (CP copper plate of the left (AS), and AA6082-T6 plate on right (RS), compared to the advancing movement of the tool through the joint-line), rigidly fixed by strap clamps, and no gap between the plates. The welding operation was done at room temperature, without any preheating, post-heating or post-cooling treatments. The tool spindle rotation was in the clockwise direction, relative to the plan view of the weld-line.

A variety of welding speeds (rotational speed; ω and advancing speed; V) were applied to validate the welding trials according to previous works [10,11,14,15,47] with different process settings. After running some tests in ω (400–1000 rpm) and V (200–600 mm/min), there were a high proportion of only partially successful welds indicating a quality problem. The issue was invariably a partially successful joint with a localised discontinuity defect through the weld-line. To evaluate the defect structure the final weld sample was produced with the trial performed in clockwise rotational speed (ω) of 800 rpm with an advancing speed (V) of 400 mm/min in the travelling direction. Schematic of the welding process and interaction between the tool and the workpieces are shown in Figure 2.

Sample preparation

The Al-Cu welded plates were 6 mm in thickness. The welded plates were wire cut by an electro-discharge machine across the failed weld-seam areas on different cross-sections, perpendicular to the welding direction. The weld length from the edge of the plate until the centre of the failure area was approximately 45 mm. Individual samples cut were about 20mm in width, and 5-20mm in length (6mm thick).

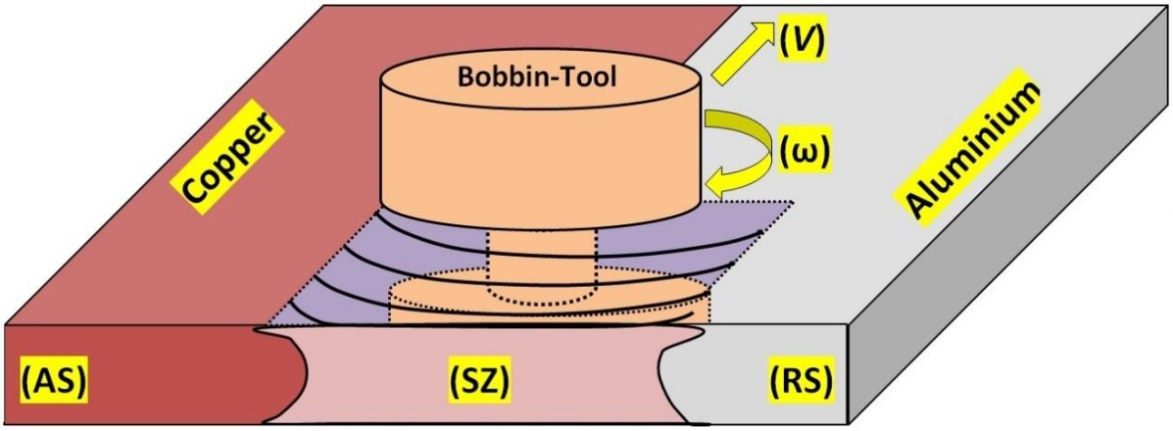

Fig. 2. Schematic of the BFSW process; the bobbin tool in interaction with the AA6082 T-6 and CP copper *plates*

For ease of handling, the samples were mounted in thermoplastic resin, and then ground using silicon carbide (SiC) papers of 180-grit, 400-grit, 600-grit, 800-grit, and 1200-grit fitted on a rotating wheel disc, spinning at 200 rpm. Deionized (DI) water was used as a lubricant during grinding, and samples were rotated in 90-degree iterations till all scratches from the previous grit vanished.

The micro-polishing was done using a micro-cloth pad in a series of 9-3-1 μm diamond pastes. Final polishing was done using a 0.06 μm micro-cloth pad at 150 rpm and 5 lbs/sample for 5-15 minutes, using a Buehler brand MasterMet colloidal silica. Samples were rinsed with cold water, ethyl alcohol, and dried under warm air. The mirror-surface was observed under an optical microscope after each polishing round or as deemed necessary.

Optical microscopy (OM)

The prepared cross-section samples were examined under an optical microscope (Olympus Metallurgical Microscope, Tokyo, Japan) using polarized exposure. Due to the contrast of colour between the CP copper and aluminium alloy, etching was shown to be unnecessary for this study, as the flow patterns within the BFSW weld region were demonstrated clearly.

Electron microscopy

For the metallurgical analysis, the scanning electron microscopy (SEM) was used, equipped with further elemental analysis using an energy-dispersive X-ray spectrometer (EDS) detector, and the grain orientation map using the electron backscatter diffraction (EBSD) detector. The SEM observations were studied with a (JEOL 6100, JEOL Inc., Peabody, MA, USA) machine. The EDS elemental mapping for the spatial distribution of the composition and the similar point analysis of elemental weights were measured by an EDS detector (Oxford Instruments plc, Abingdon, UK), with the working voltage of 20 kV. The analysing software for processing of EDS data was AZtecLive & Ultim Max (X-Max version, Oxford Instruments plc, Abingdon, UK). An HKL Nordlys III model EBSD detector (Oxford Instruments plc, Abingdon, UK) was used to create the inverse pole figure (IPF) colouring map for the weld region.

RESULTS

Copper-aluminium overview of weld

The Al-Cu BFSW weld plate, shown in Figure 3., was examined. A continuous fracture line is observed in the middle of the weld-line, representative of the improper welding condition. Nevertheless, the weld structure can reveal the origins of the failure, identifying how the interaction between the tool and substrate results in the occurrence of structural defects. Moreover, the internal flow patterns are useful to evaluate the performance of the applied operational welding parameters and its relationship with the emergence of the discontinuity defect as the outcome of the flow failure within the weld region. Further microscopic measurements of the weld were progressed on the cross-sections of the weld. In this regard, the weld samples were selected from different sections along the weld, as shown in Figure 3.

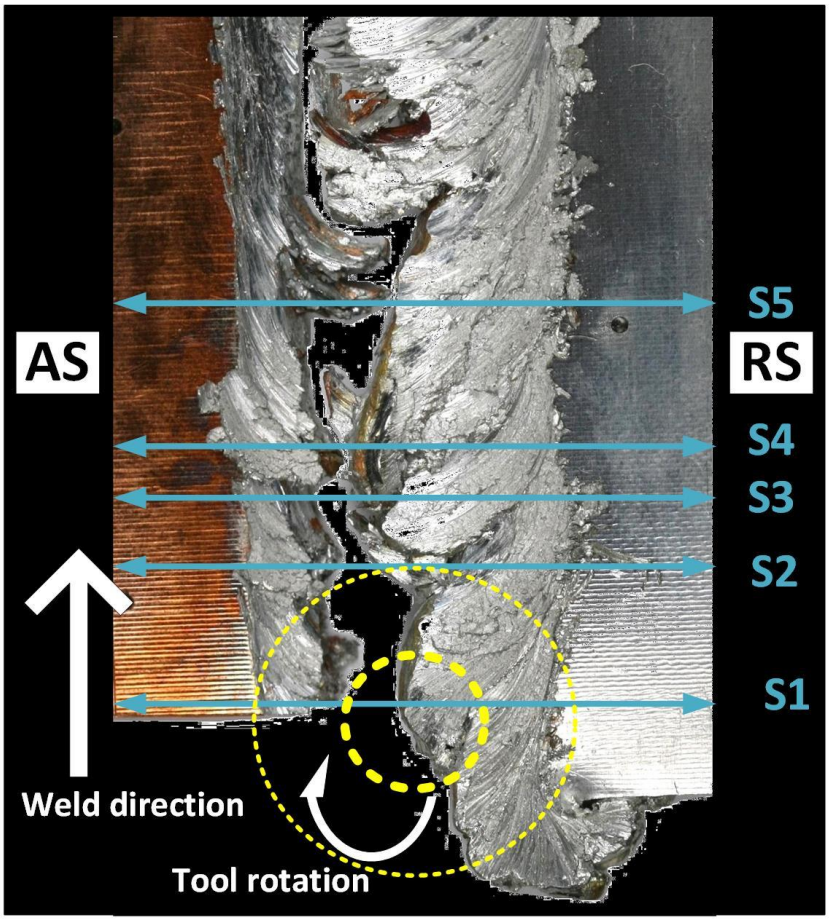

Fig. 3. Visual surface analysis of the Al-Cu hybrid BFSW weld. The top-view of the weldment; CP copper plate on the AS (left) and AA6082-T6 aluminium plate on the RS (left)

Cross-sections; Cu-side (AS), Al-side (RS)

The Al-Cu cross-sections are shown in Figure 4, according to the selected sections (S1 and S5) from the weld plate shown in Figure 3. These represent different flow patterns within the weld cross-section, as the rotating tool moves forward along the weld line. The interaction between the copper and aluminium flow layers are different on the Cu-side (AS) and Al-side (RS) of the weld.

Because of the suitable contrast between the copper and aluminium mass flows, the samples can provide a clear flow visualization without using any etchant reagents (Figure 4a). It should be noted that the investigation of the defective welded joint can provide a better visualization of the flow failure through the weld-line. Figures 4b-d reveal some more microscopic details of the microstructure for the stirring zone of the hybrid weld, with a focus on flow mechanism and metallurgical explanation of the welding.

Figure 4b shows the SEM micrograph of the selected frame of the mid-SZ from Figure 4a. to evaluate the hybrid weld texture, the IPF colour map and the corresponding EDS elemental map of the mid-SZ are shown in Figures 4c and 4d, respectively.

The grain orientation map (Figure 4c) illustrates an equiaxed grain morphology in mid-SZ with a random grain orientation distributed through the intermixed layers of the Al-Cu phase texture. The homogenised microstructure in mid-SZ can be attributed to the mechanical stirring of the pin causing a uniform grain fragmentation and subsequent plastic deformation.

The corresponding EDS elemental map (Figure 4d) shows the formation of a variety of the intermetallic compounds within the interlayer transition region of the weld. The large lumps with similar composition are the macroscopically visible feature (over 1000μm) extending towards the centre of the weld.

Key findings are that there is an interlayer mixing between the Al- and Cu- mass flow layers during the stirring action. The EDS analysis confirms that this results in the in-situ formation of the intermetallic phases within the hybrid weld structure. The further development of the IMCs formation can intensively affect the strength of the weld, causing the flow failure during the tool advancement through the weld-seam. The IMCs has significant implications for the welding process because the brittle phases presumably restrict the reattachment of dissimilar flow resulting in a discrete metallurgical bonding.

In cross-sections in Figure 4e, the weld structure shows large internal cracks in the middle of the stirring zone, leading to the spontaneous fracture, and subsequently, the failure of the final weldment. The material loss at the position of the failure in mid-SZ, interrupt the flow-lines at the middle of the weld region. However, the deposited dissimilar flow layers at the AS and RS borders, and near the top and bottom surfaces near the sub-shoulder regions, can give some useful insights about the flow mechanism during BFSW processing of the dissimilar welds.

A general observation of the progression along the weld is that there are large pieces of copper that are firmly bonded to the aluminium (from mid-SZ towards the RS). Within these are regions of pure copper and areas of intermetallic, which could indicate a well-stirred zone. There are also large areas of IMCs underneath the shoulders that are predominately aluminium with small fragments of copper. All these IMCs have a lamellae structure to them, and this is especially pronounced under the shoulders (upper and lower surfaces). Multiple alternating large bands of copper and aluminium are also noticed throughout the weld region near the AS border. The general trend of flow features apparent on the Cu-side at the AS border can be explained as (i) the enlarged lumps of the solid copper, intact up to the hourglass border, and (ii) the presence of the thin layers of aluminium rich material observed at the proximity of the sub-shoulders. There is also a fragmented area inwards of the hourglass border, with poor adhesion.

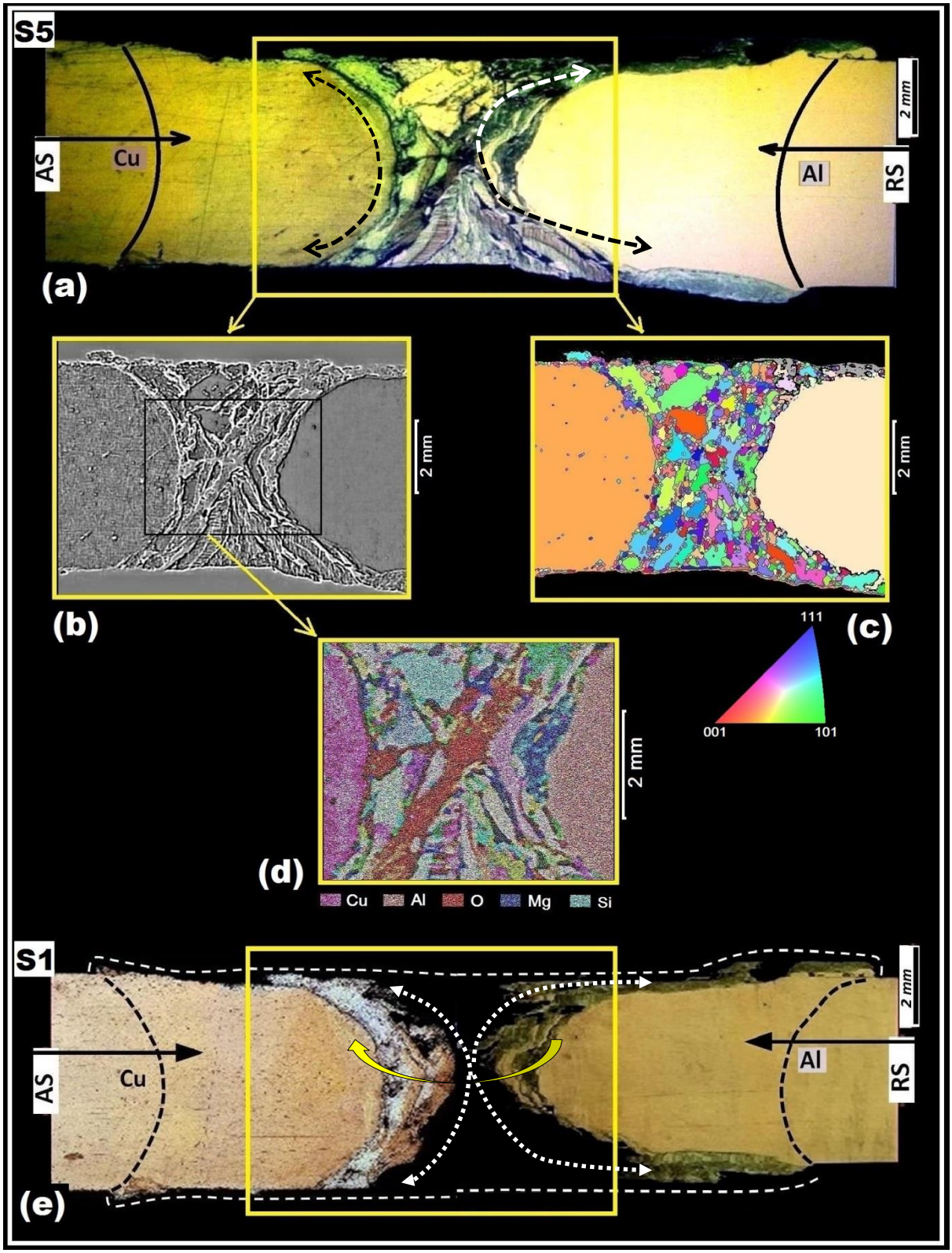

Fig. 4. Cross-sections on the hybrid weld of Al-Cu BFSW, representative of dissimilar flow interaction between the aluminium and copper mass layers; Cu-side (AS) and Al-side (RS).(a) weld cross-section from S5-sectionin in Figure 3, (b) SEM micrograph of mid-SZ, (c) IPF EBSD map of mid-SZ, (d) EDS elemental map of mid-SZ, (e)weld cross-section from S1-sectionin in Figure 3

Detailed examination of regions of interest through the weld cross-section

The stirring zone has multiple morphological features that can be identified in Figures 5-10: large deposits of material, both Al and Cu, a stirred area at the sub-shoulder regions with fragmented material within it (intermetallic region), large voids, and the formation of lamella patterns as the intermixing between the intercalated layers of Al and Cu.

Al-side (on the RS border)

Figures 5 and 6 show the formation of intermixing stirring zone at the Al-side of the weld towards the RS border. Two main microscopic features of the material formability at the SZ are: the IMCs regions near the sub-shoulders (Region 1, Figure 5), and deposited lamellae patterns in a large Cu fragmented pieces (Region 2, Figure 5).

The Fragments of copper particles are observed in an Al matrix near the shoulders. This formation of material near the shoulders seems to be consistent throughout the weld sections, as highlighted as the Region 1, in Figure 5. The lamellae formed swirl patterns but are bounded in the Cu matrix and do not extend to the Al matrix. The small copper particles have finer lamellae structures, which could be interpreted as material that has been processed multiple times around the tool. Similarly, in Figure 6, IMCs and lamellae formation as observed are mostly visible in the middle of the stirring zone and far from the RS border; where the fragments of copper particles are noted to be situated in the Al matrix. The large pieces of copper near the RS border (Al-side) appear with a formation of lamellae structured intermetallic compounds within them. However, the deposited pieces of copper at the middle of the SZ, are deposited with large discontinuity crack between the pin-position and the Al-matrix. This can be related to the viscoplasticity of the Al- and Cu- mass layers, during the stirring, and differences in density and thermal expansion of them within the dissimilar joint.

Cu-side (on the AS border)

Figure 6 showed the large pieces of copper are gradually detached from the base metal in the SZ, approximately where the pin is crossing through. Simultaneously, the stirred aluminium appears to be attached to the Cu base metal, connecting to the copper pieces, though still showing large voids in between (Figure 7). Copper particles in an aluminium matrix are commonly observed, but the reverse is not often found. Figure 8 shows Al pieces found in a Cu matrix (Region 1, Figure 7). These are larger in size compared to what is seen of the Cu particles in an Al matrix, and it appears they seeped in through the cracks in the copper matrix rather than being shaped in it. Moreover, small copper particles (less than 10μm in size) appear to be distributed in the Al matrix (Figure 8, Region b). In Figure 9, a clear division is seen between the large pieces of copper and aluminium. What is more apparent is the lamellae layers of copper, dispersed within the Al-matrix (Region 2, Figure 7). These individually separated copper pieces in the Al-matrix can be a plausible place for the formation of IMCs.

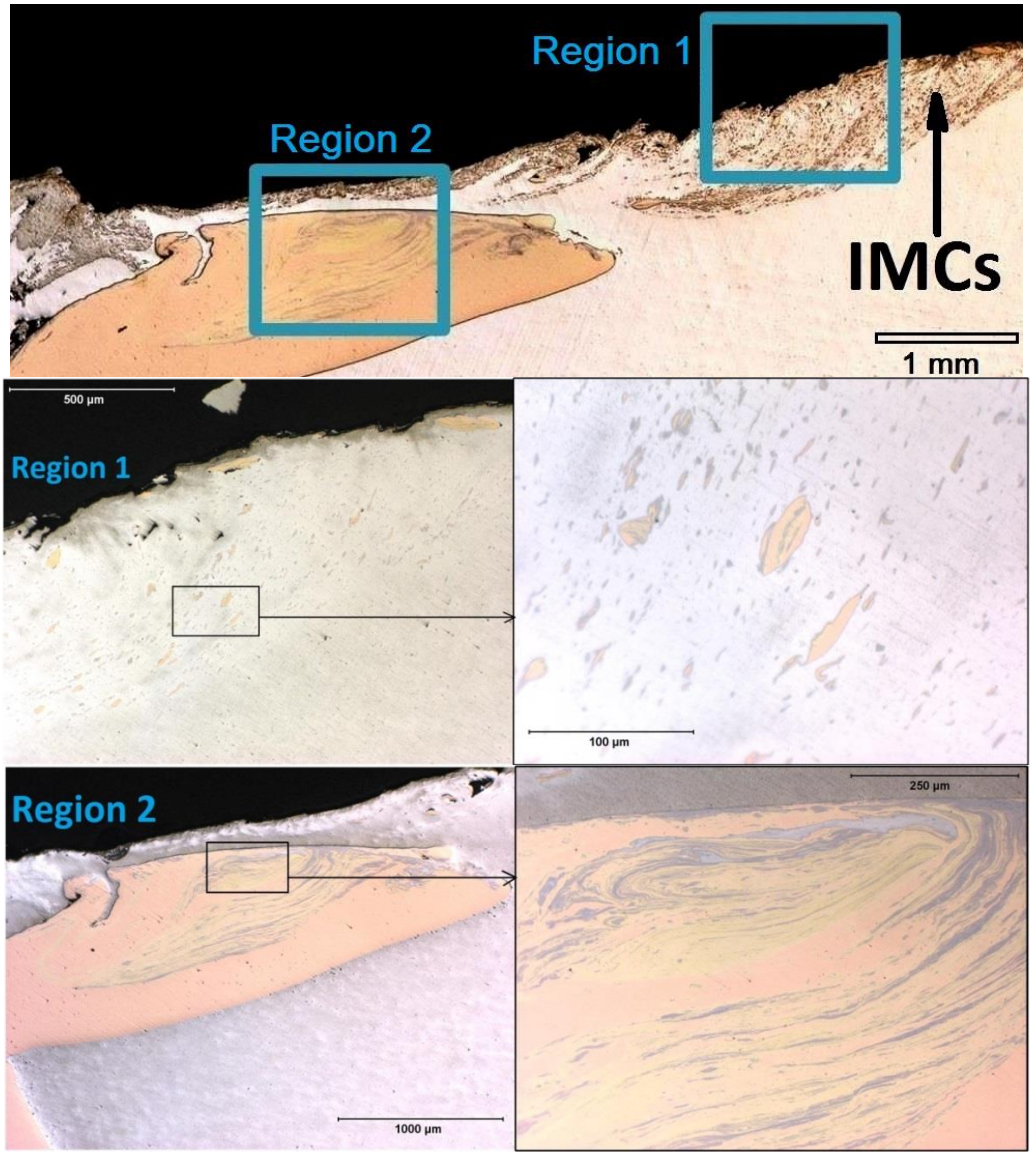

Fig. 5. Optical micrograph of the weld cross-section from Al-side location (sample from S2-section in Figure 3). Regions of interest. Regions 1; formation of intermetallic compounds (IMCs). Regions 2; lamellae formation in a Cu packet

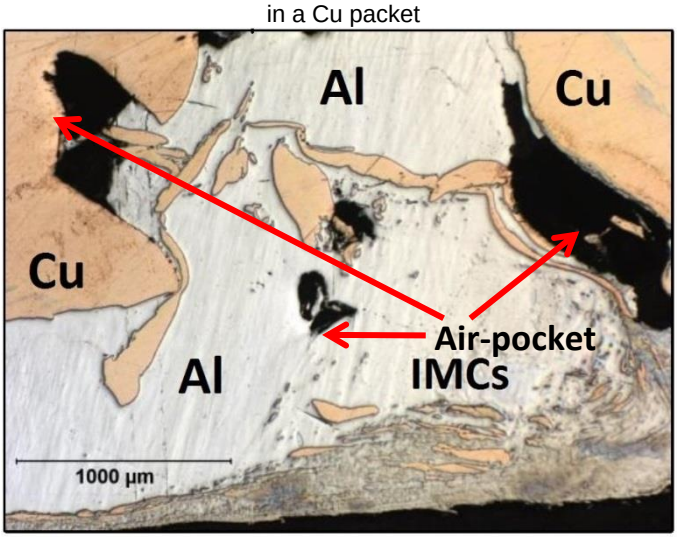

Fig. 6. Large copper particles in the mid-thickness region. Al-side, (sample from S3-section in Figure 3)

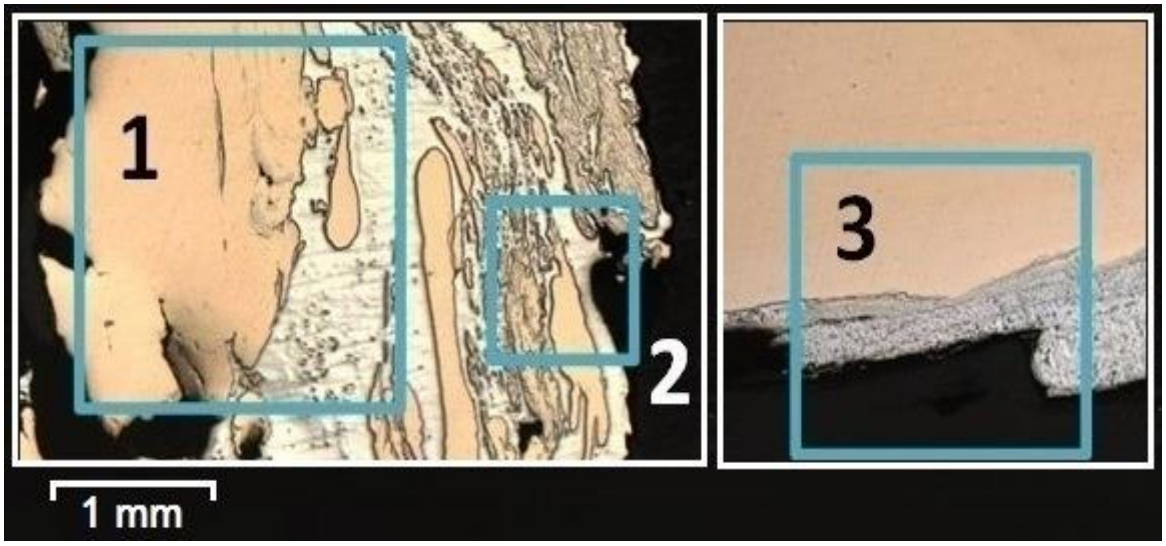

Fig. 7. Advancing side, Cu-side, (sample from S4-section in Figure 3)

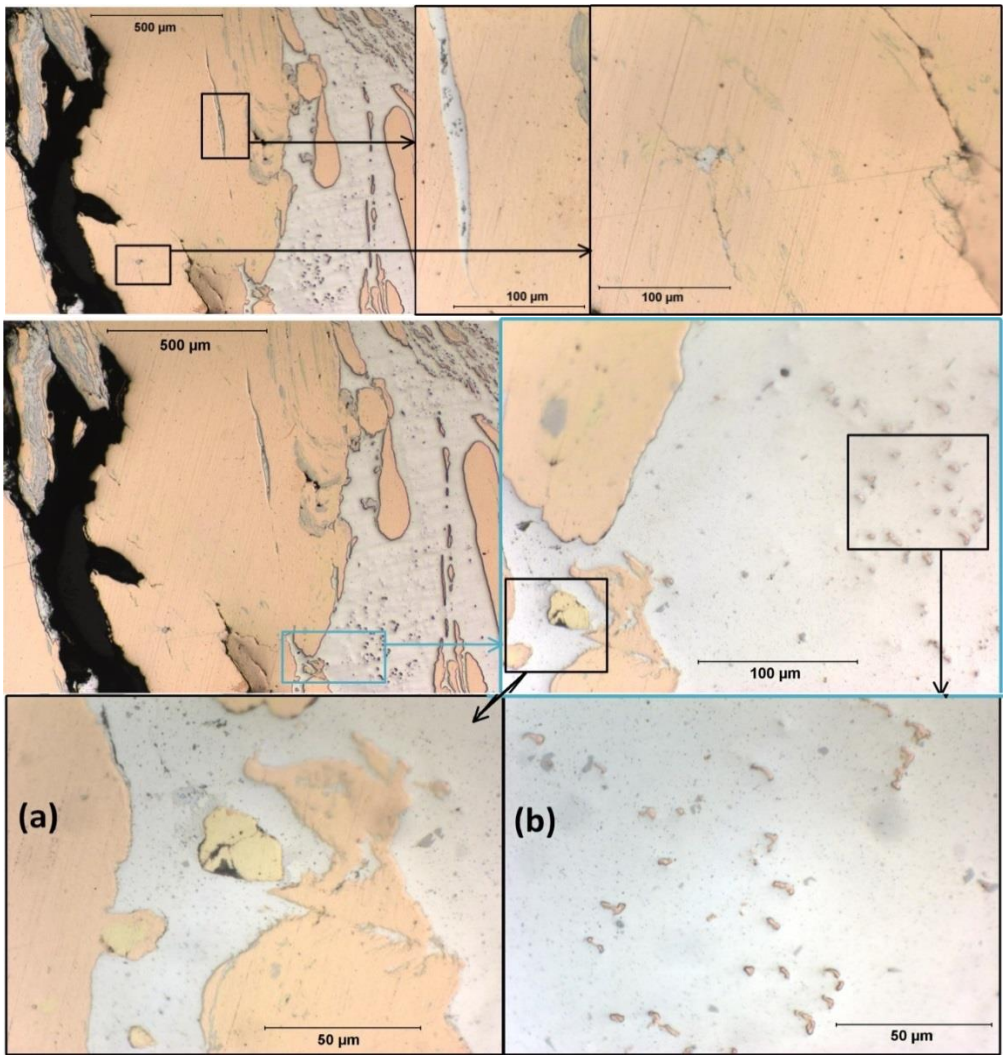

Fig. 8. Al particles in Cu-side (Region 1 from Figure 7). (a, b) Cu particles in Al matrix

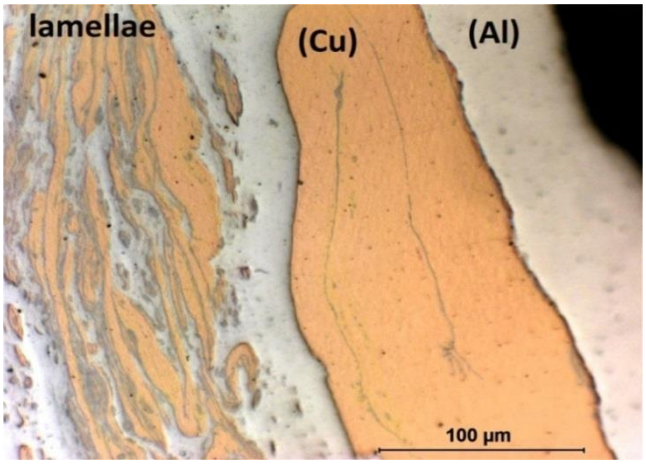

Fig. 9. Cu lamella formation in between Cu- and Al- large particle lumps, (Region 2 from Figure 7)

The sub-shoulder region on the Cu-side of the SZ (region 3 from Figure 7) indicates fragmented particles pattern similar to the Al-side (Figures 5 and 6). The magnified micrographs of the sub-shoulder region of the Cu-side are shown in Figure 10. An aluminium mix is observed integrated with the pure copper matrix through a structured lamella division. As the sub-shoulder pattern moves away from the centre, the stirred aluminium changes from a lamella structured formation with the copper, to having copper particles within the aluminium matrix. The small copper particles show signs of intermetallic formation within them. This seems to be a consistent formation as shown in the Cu cross-sections taken from different weld sections (observable in Region b, Figure 8). Cracks are also noticed in this area, as it is appearing between the lamellae formed structure and the IMCs distributed particles.

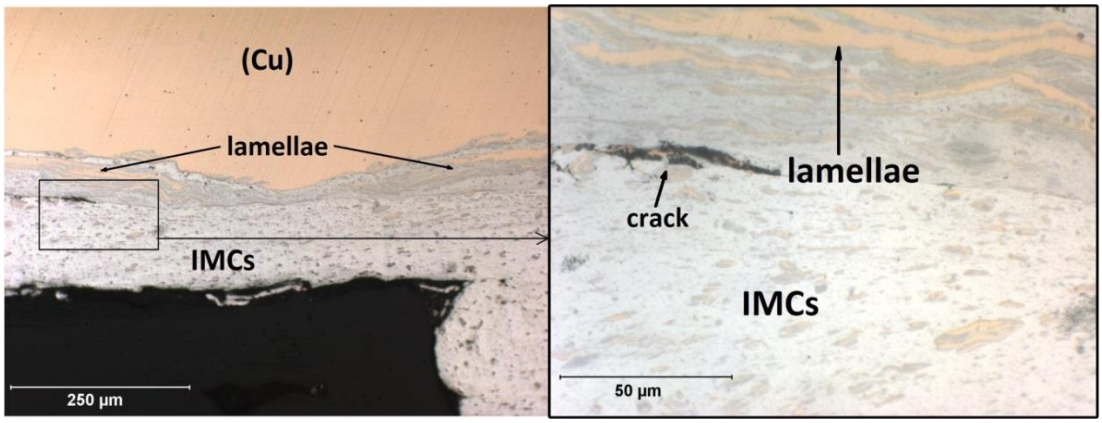

Fig. 10. Sub-shoulder region from Cu-side of the stirring zone, located on the AS border of the weld. (Region 3 from Figure 7)

Electron microscopy (IMCs)

For further evaluation of the microscopic features driven from the flow interaction, the SZ was analysed by the SEM and relevant EDS mapping.

Based on the observation of the optical micrograph image, the small particles in the Al matrix appear to us as Cu pieces; this has been confirmed by the SEM-EDS results (Figures 11-14).

Figure 11 demonstrates the microscopic details of the SZ with a focus on the sub-shoulder region, where the dispersed Cu-based particles from the AS passing through the SZ, with a higher concentration at the sub-shoulder region. The relevant EDS elemental map

(Figure 12) confirmed that copper is the main element of the composition of these dispersed particles. This is following the nature of the stirring action which provides a stirred mass without uncontrolled reaction between the mass compositions.

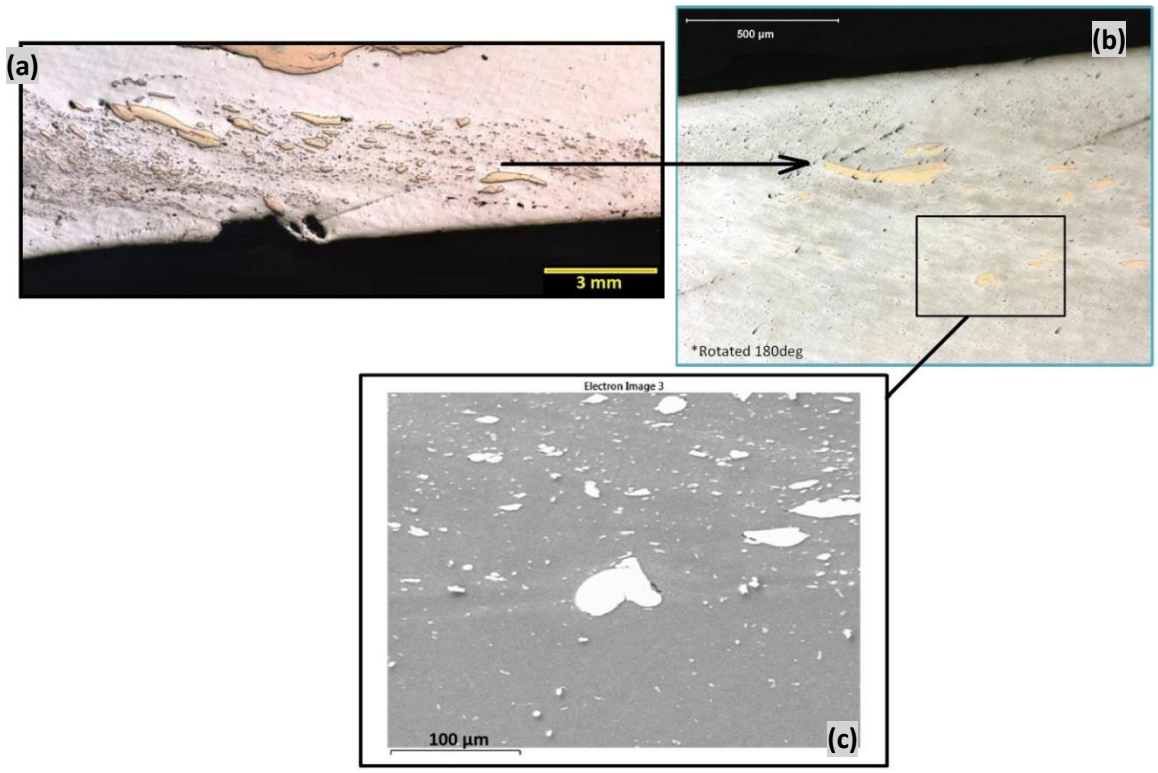

Fig. 11. SEM image of IMCs situated at the sub-shoulder region from the Al-side (near the RS border). (a) the weld cross-section, near the Al-Side at RS (OM micrograph), (b) sub-shoulder region; IMCs-rich zone (OM micrograph), (c) sub-shoulder IMCs partiles in higher magnification. SEM micrograph

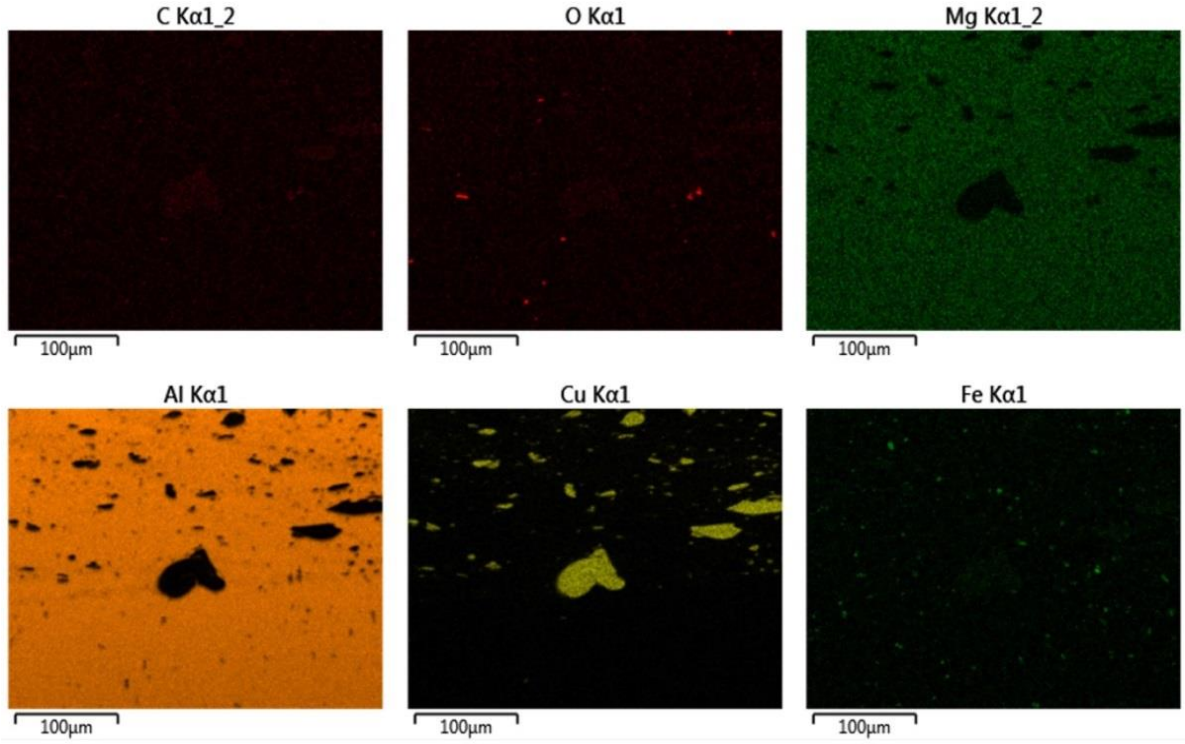

Fig. 12. Results of the EDS elemental map, for the sub-shoulder IMCs particles, shown in Figure 11c

The stirred mass at the mid-SZ region shows a layered deposited pattern, typically named as the lamellae swirling pattern. This is a direct outcome of the stirring at the proximity of the pin position. The shearing induced by the features of the pin threads could be responsible for this layered deformation. The changing of the colour between the copper and aluminium through this pattern implies the formation of an intermetallic layered band. To confirm this hypothesis, observed lamellae patterns were analysed by EDS elemental mapping and point mapping tests (Figures 13 and 14, respectively) to measure the chemical composition of the mass. The EDS elemental map (Figure 13) shows extreme mixing of the mass between the Al and Cu, as the colour contrasts these two elements it illustrates overlapping, with similar colour contrast. The elemental point analysis of the lamellae pattern also confirms that, although this region belongs to the Cu mass, a suitable level of mixing of Al alloy particles was observed from the analysed layers. Therefore, efficient mixing of the Al and Cu in this lamellae region has occurred.

A lamellae formation in a Cu matrix was also observed using the SEM. The EDS elemental map results show that both Al and Cu are present, but are in the form of IMCs. The elemental point analysis (Figure 14) presents findings of the percentage of individual materials; it shows that Cu is the major material, while the presence of carbon (11.4% in wt%) is also high which can be related to the coating layer before the SEM measurements.

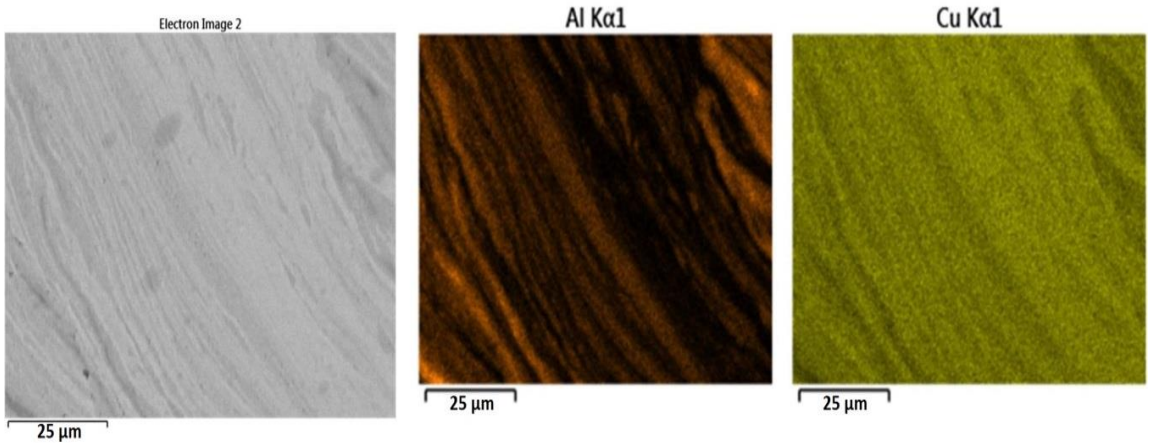

Fig. 13. The EDS elemental map for the lamellae pattern formed within the copper lumps within the stirring zone, shown in Figure 9

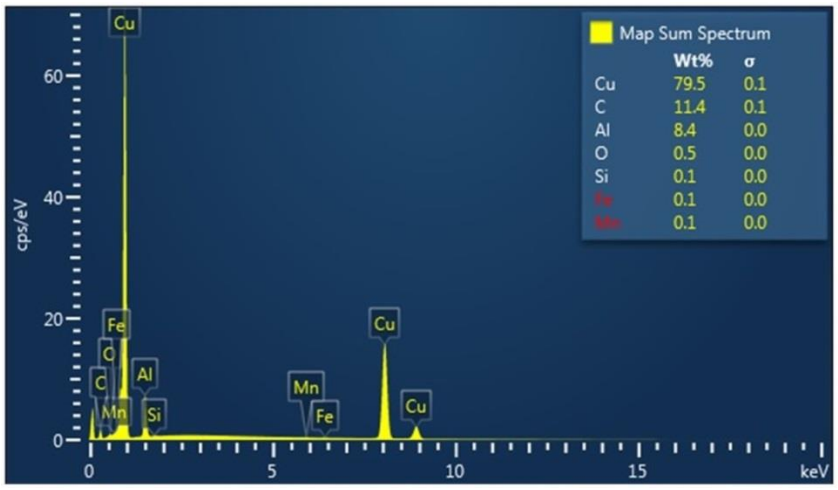

Fig. 14. The EDS elemental point analysis for the lamellae pattern in Figure 13. The chemical composition of elements is listed by the weight percentage

DISCUSSION
towards a theory for dissimilar BFSW welding

Metallurgy of the weld

The dissimilar bonding structure in Al-Cu hybrid joint in the FSW process as has a specific microstructure within the stirring zone of the weld structure, containing the IMCs [48]. The external heat input and mechanical stirring action cause a nonequilibrium deformation assisted by the adhesive transferring of the mass flow around the tool position [48,49]. Moreover, the dynamic recrystallization and mechanochemical precipitation are the additional post-welding solid-phase reactions whereby result in the formation of the intermetallic compounds within the Al/Cu interface [4]. It should be noted that in addition to the process temperatures, the composition of the in-situ synthesizing IMC phases is depended on the local Cu-content during the intermixing process [50]. This is also clear in the morphology of the interlayer bonding by a different colour between the Al and Cu- mass flows. Unlikely, the intermixing solid solution at the middle of the stirring zone reveals a more homogenised plastic deformation between the parent metal phases. Furthermore, the formation of the eutectics facilitates the adhesion bonding within the stirred solid solution.

In this work, the microscopic measurements of the Al-Cu hybrid BFSW weld was investigated by optical and electron microscopy. The micrographs from the SZ both in Al-side and Cu-side identified different flow-based intermixing layers, IMCs compounds, and intercalated lamellae morphologies of swirling bands within the dissimilar weld breadth. The EDS analysis characterized the chemical composition of the Al-Cu complex structures of IMCs and lamellae layers, found within both the AS and RS borders of the dissimilar weld. At most locations, these microscopic features are observed as a mixture, which makes it hard to accurately recognise the specific regions for the original formation of each within the SZ. However, the IMCs are mostly detected in the sub-shoulder regions, between the fragmented Cu particles, or between the swirling lamellae layers.

Although the cross-section micrographs revealed the details of the intermixing patterns as the result of the plastic deformation in the interaction between the tool and the Al-Cu substrates, the stirred structure still could not achieve a fully homogeneous mixture. This is the main challenge during the BFSW processing of the dissimilar Al-Cu weldment. More specifically, regarding the copper mass entered into the SZ, the interaction between the plastic layers shows large pieces of copper-lumps with lamellar intercalated features deposited within the weld structure towards the RS (Al-side). Far from the middle of the stirring zone, the fragmentation of Cu particles at the sub-shoulder leads to formation of a vortex-shaped mixture near the top and bottom surfaces of the cross-section, the material is rich of IMCs phases.

Formation of large voids and cracks within the SZ were also inevitable in observed processed cross-sections. These discontinuity defects mostly occurred at the boundary layers between the Cu and Al interface. This originated from the inefficient or inadequate mixing plastic flow between the Cu and Al mass layers entering into the SZ, from the AS and RS borders, respectively.

Moreover, the different density of the Al and Cu mass, and the brittle nature of the IMCs phases distributed through the SZ can also intensify the formation of the discontinuity layers between the dissimilar deposited layers.

Irregular distribution of Al- and Cu-layers, and formation of IMCs-rich morphology (flake-shaped phase) causes insufficient refilling during the mass-circulation at the proximity

of the rotating tool. Therefore, the inadequate intermixing of the flow layers interrupts the integrity of the flow deposition at the trailing edge of the tool. Therefore, the weld-seam forms with internal flow-based defects, e.g. voids or cracks.

Flow mechanism around the rotating tool

The main challenge during this work was to obtain a defect-free joint for comparison. However, existing weld defects within the weld seam can explain the defect formation mechanism with a flow-based approach in relationship with the tool features and interaction between the tool and substrate.

The geometric details of the bobbin tool, (including threads, flats and grooved scrolls), can affect the flow regimes during the stirring process [14,15]. The threads and flats drive a lateral motion around the pin, vertically pumping the material inwards and avoiding from spilling. Moreover, the inward-flowing spiral grooves on the shoulder surfaces also feed the plastic flow inwards, providing a circulation towards the centre of the stirring zone. These provide more homogenized mass transportation, with a better engagement between the rotating tool and the substrate materials [11].

During the stirring of dissimilar mass flows, the complex materials transferring around of the tool creates an unfilled zone at the centre of the stirring zone. This is because of the insufficient intermixing during the refilling process at the trailing edge of the tool, leading to emerge an empty space in the form of a continuous cavity defect. Moreover, by the moving of the plastic flow from the advancing edge of the tool to the trailing edge, the transported materials can be dispersed to the outwards of the stirring position, in which causing the material loss at the weld region.

The transportation of the copper mass packets around the pin was observed in a unique material flow pattern, not previously identified in the literature. Based on the microstructure observations, here, we propose a flow-based explanation for the mass flow transportation mechanism around the rotating pin. The sequence of the flow mechanism is demonstrated in Figure 15.

Reference to Figure 15a; the clockwise tool rotation begins the mass flow at the AS by grabbing copper mass via pin features (threads-flats). The thread's-flat features of the pin provide an efficient frictional condition at the surface of the rotating pin, which increases the adhesion of the material to the pin and its transportation and release, to pack the material towards the retreating side. As the tool travels through the interface, the copper mass at the leading edge of the pin experiences transverse transportation towards the RS. Simultaneously, the aluminium mass at the RS undergoes a reverse flow towards the trailing edge of the pin, opposite to the tool travel direction, see Figure 15b. The relocation of the aluminium mass, makes extra space for the yielded copper mass to have more lateral thrust towards the RS to refill the stirred aluminium into the primary position at the AS. In this regard, the features of the flat pin would capture more volume of the copper mass and contribute to mass transportation. The copper mass packet would move from the AS to the RS of the pin; it is now surrounded by the aluminium mass (Figure 15c). The extra mass-circulation around the pin intensifies the thrust of the copper mass packet stuck to the pin and eventually separates it from the position of the pin.

Consequently, large volumes of the copper packets get deposited at the retreating side Figure 15d, due to the combination of the clockwise rotation and forward movement of the tool which creates two opposite flow directions at the RS of the pin. The rotating pin continues the stirring action whereby the mass-circulation continues from the retreating side to be deposited at the advancing side However, the deposition of the copper mass packets, swept at the RS, makes it hard for the pin to laterally displace them again to the backside of

the pin to complete the circulation towards the RS. This can cause a deficit in the material flow at the trailing edge of the tool in the form of incomplete RS-to-AS mass transportation. This is where the loss of the mass occurs near the AS. At the same time, the further tool travel consolidates the stirred mass deposited behind the tool, with a discontinuity defect indicating a weak joint.

Based on the flow mechanism in the BFSW process, there are two main regions induced by plastic deformation that identify as part of the SZ.

(1) The sub-shoulder region; where the top and bottom shoulders are acting upon the workpiece, these sub-shoulder regions are induced by plastic deformation caused by the tool rotation. The typical flow features induced by the top and bottom shoulders are demonstrated in Figure 7 and Figure 13, respectively.

(2) Mid-thickness region; which undergoes a dominant flow induced by the pin action. The most evident flow feature in this region is the lamellae-shaped swirling flow patterns within the copper mass deposited towards the Al-side (RS), see Figure 8 and Figure 12. This flow complexity can be related to the geometric features of the pin [51], specifically the threads which can induce a micro-circulation through the stirred layers of the mass [52].

Besides the mechanical friction action from the shoulders, the shoulder surface has a spiral scroll feature that would cause more localised deformation near the surface of the workpiece. The outcomes can be observed as a turbulent flow regime at the sub-shoulder areas with fine mixing of Cu particles in the Al matrix. The uniform dispersion of the Cu particles at the Al-side (RS) is evident; this can be attributed to the deformation induced by the shoulder scrolled surface, as well as the deformability of small pieces of copper. This formation aligns with another work [4], where the FSW tool offset towards the Al-side meant that smaller copper particles are mixed in and a better interface is created.

The EDS results shown in Figure 15 imply that some shredded Cu particles exist without reaction with theAA6082-T6 alloy. This can be attributed to the fast cooling at the sub-shoulder region, where the mass is in contact with the free-air once the tool leaves the location of the stirring action. To identify the history of the dynamic recrystallization at the sub-shoulder region, further metallurgical characterisation is required to analyse the composition and microstructure of the Cu dispersed particles with a focus on the plausible formation of the intermetallic phase at the interface of the Cu-Al phases. This is an interesting subject for future studies, as the larger copper particles contain some lamellae-shaped pattern in the middle, which indicates presence of intermetallic compounds.

The clockwise transverse transportation of the plasticised mass from the AS towards the RS around the proximity of the rotating tool causes a circulating flow condition which can be responsible for the lamella pattern [53,54]. As the generated heat at the middle of the SZ is in a higher rate compared to the sub-shoulder region [55], there are more suitable conditions for atoms to interact together and form intermetallic compounds, such as the ones within these lamella regions. This has been measured in Figures 12-14, confirming the existence of the intermetallic compounds at the position of the lamella patterns.

Previous studies have shown that Cu malleability is not enough to achieve a proper mechanical stirring (Cu requires a homologous temperature close to 0.8), hence detached large Cu particles would be harder to flow in the Al matrix, this is shown clearly at the mid-thickness region (see Figure 6).

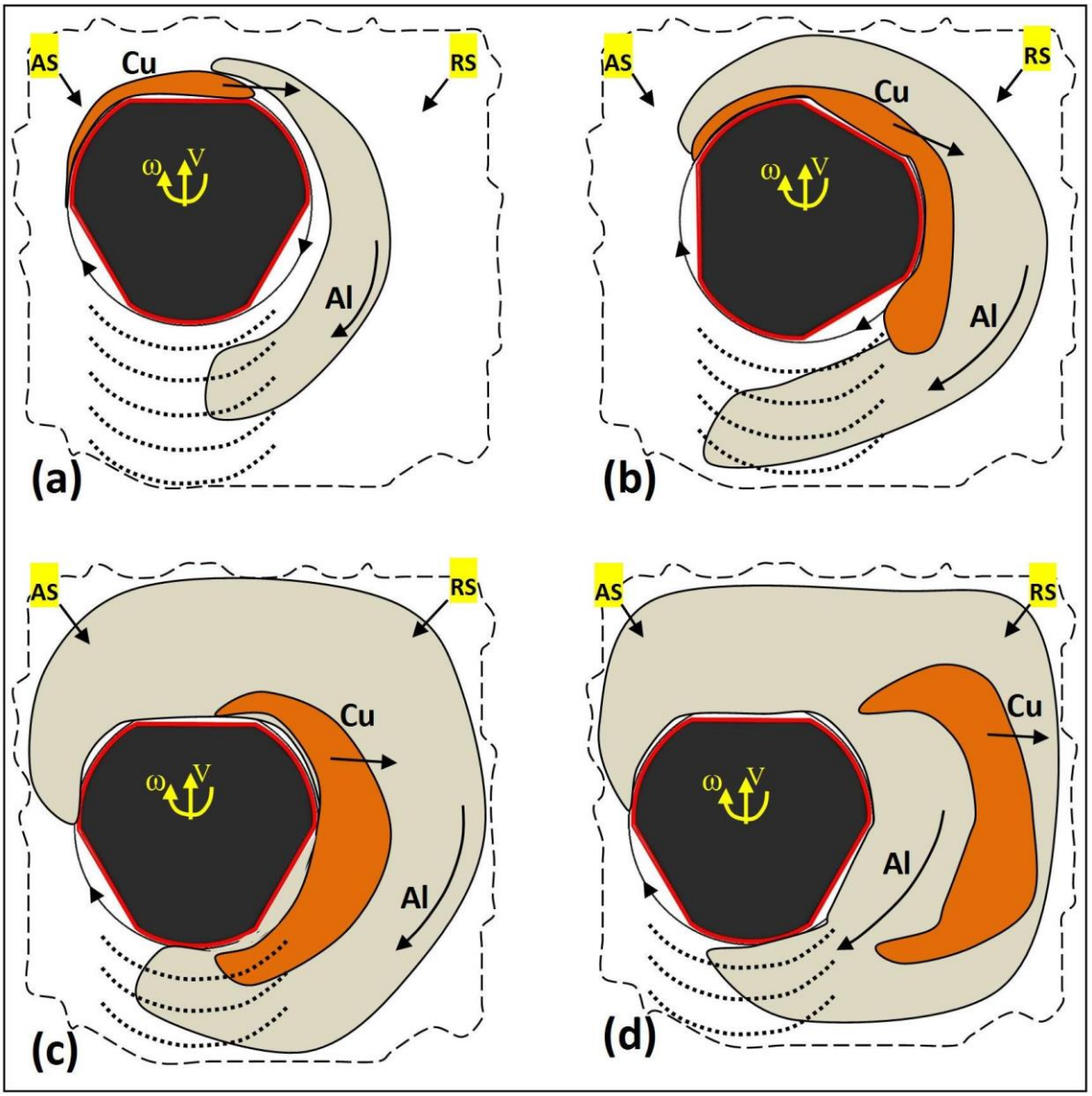

Fig. 15. Schematic of the Al-Cu mass flow patterns; (a-d) Sequence of the mass flow transportation around the rotating pin in interaction with the Al-Cu plates

Implications for dissimilar welding processes

The difference in density, strength, and the viscoplasticity of the stirred materials would cause defects in solid-state welding. The chipped formation of the large copper pieces embedded within the Al matrix is an example of defect due to difference in deformability.

The weld examined in this research showed a discontinuity line at the interface of the weld. This could mean that the applied welding operational parameters led to the failure of the weld. The origins of the welding failure can be attributed to the insufficient flow circulation at the SZ to transport the Al and Cu in a uniform flow path. To obain the flow integrity, a homogenous mixing regime at the trailing edge of the tool is necessary, where the mass layers are depositing as the bonding material, and it is needed to be protected from the dispersing before actual consolidation of the weld seam.

Combined flow visualisation on transverse and plan-view sections of weld samples can be useful in a better understanding of the discontinuity defects emergence within the mass flow layers [56]. The material transformation and subsequent consolidation during the

refilling action can be also evaluated more precisely in terms of parameters such as welding speeds (rpm and feed rate) and the tool geometry (threads, flats, scrolls) [13]. The influence of the tool profile in the stirring action can be presented within the microstructural observations from the different regions of the dissimilar joint, exposing the flow patterns of the plastically deformed bonded area. Regarding the Al-Cu joint, the flow observations revealed that the Al-mass layer being softer compared to the Cu-mass layers, which has better viscoplasticity behaviour under the stirring condition. Therefore, within the intermixing bonding area, the Al-mass layer transforms in a greater amount, occupying the emptied space at the initial position of the Cu-mass during the refilling process. However, the existing inconsistency between the interlayer flows makes some difficulties in an insufficient mixing of the transported materials at the trailing edge of the tool. Thus, the improper mass consolidation resulting in discontinuity defects within the structure of the Al-Cu dissimilar joint.

There are some possibilities which we believe can affect the stirring action to occur the flow failure. Stirring is a mechanical action leading to plastic deformation of the workpiece material, but the macro observation of the cross-sections shows a poor deformation pattern for the Cu material deposited in SZ. The existence of some large chunky-shaped pieces of copper suggests poor deformability of the Cu mass under the applied operation condition. Higher density and work-hardening strength of the copper compared to the Al-alloys can explain the inconsistency in the deformation of the Cu under the same stirring condition induced by the tool. Therefore, the unsuitable viscoplasticity of the Cu stirred mass can lead to failure of the plastic flow transportation between the AS and RS at the position of the tool rotation.

To make successful Al-Cu welds the next step can be the control of the IMCs formation as a limitation in weld texture. Furthermore, the failed flow and discontinuity defect might be attributed to the uncontrolled coarse IMCs. As a consequent, the embrittled compounds deteriorate the strength of the weld structure. In this regards, one of possible solutions is to apply the controlled welding speeds and frictional heat to optimise the plastic flow and the subsequent intermixing mechanism between dissimilar plasticity regions of Al- and Cu.

Implications for future work

Further analysis of the current samples can be conducted. Studying the grain boundaries using the developed metallographic etchants, as well as additional analysis using the EBSD method, would contribute to understanding the weld.

Compared to the symmetric configuration of the bobbin-tool, the conventional-FSW resulted in asymmetric deformation [14,47]. Moreover, by replacing the backing anvil (in conventional-FSW) with a rotating bottom shoulder, the BFSW process has a better capability for the elevation of heat generation [11,47]. This can improve the material transportation during the stirring, resulting in better intermixing between the Al- and Cu- plasticised mass flows. However, the elevated temperature can have some unpredicted effects in the uncontrolled formation of the IMCs phase in dissimilar Al-Cu welding.

The mass flow model for the dissimilar joint also can be visualised by the analogue modelling of the multi-layered plasticine [53,54]. The transportation mechanism inside the plasticity region can be followed by the combined flow lines of the analogue model corresponding to the complexity of the tool profile. Consequently, the layer-by-layer movement pattern of material in analogue model can reveal any potential position of the local failure in the intermixing flow, where during the insufficient stirring action emerges the discontinuity defects.

Possible future research topics that might be helpful for better understanding BFSWing of dissimilar materials could be regarding the material processing mechanism in dissimilar Al-Cu BFSW processes, and characterisation of other regions of the weld can be useful to build a

more comprehensive theory. Further analysis of the intermetallic compositions in a different region of the weld can also elucidate the metallurgical aspect of the BFSW welding process for dissimilar joints of Al-Cu.

SUMMARY

This research inspected a dissimilar hybrid butt-joint of Al-Cu processed by the BFSW technique. This study aimed to examine the flow-based features of the materials mixing occurring during the stirring mechanism in the weld region. The colour contrast between the aluminium and copper provides a suitable level of flow visualisation without applying any etchant reagent for the cross-section of the weld. This allowed the microscopic measurements to study the flow features of the weld in a direct scheme. The microscopic details of the weld region were analysed by the metallographic measurements using optical and electron microscopes. The observed flow features of the Stir Zone (SZ), and the trace of the intermetallic formation confirmed the mixing of the Aluminium and Copper under the rotating bobbin tool. However, inconsistency of the flow regimes and insufficient engagement of the tool and substrate led to the failure of the weld by creating a discontinuity near the Cu-side. By comparing the internal microflow patterns between the samples of the broken joints, we can look for signs of what may improve the welding process. The origins of the flow failure also elucidated the interaction between the tool and substrate during the dissimilar stirring action.

ORCID iD:
Abbas Tamadon https://orcid.org/0000-0001-7367-4207
Dirk J. Pons https://orcid.org/0000-0001-7141-0291
Don Clucas https://orcid.org/0000-0002-6724-3037

REFERENCES

1. Mehta, K.P.; Badheka, V.J. A review on dissimilar friction stir welding of copper to aluminum: Process, properties, and variants. Materials and Manufacturing Processes 2016, 31, 233-254.
2. Sharma, N.; SIDDIQUEE, A.N. Friction stir welding of aluminum to copper—an overview. Transactions of Nonferrous Metals Society of China 2017, 27, 2113-2136.
3. Fonda, R.; Knipling, K. Texture development in friction stir welds. Science and Technology of Welding and Joining 2011, 16, 288-294.
4. Xue, P.; Ni, D.; Wang, D.; Xiao, B.; Ma, Z. Effect of friction stir welding parameters on the microstructure and mechanical properties of the dissimilar al–cu joints. Materials Science and Engineering: A 2011, 528, 4683-4689.
5. Threadgill, P.; Leonard, A.; Shercliff, H.; Withers, P. Friction stir welding of aluminium alloys. International Materials Reviews 2009, 54, 49-93.
6. Thomas, W.; Nicholas, E.; Needham, J.; Murch, M.; Temple-Smith, P.; Dawes, C. Friction stir butt welding, international patent application no. PCT/GB92 Patent application 1991.

7. Thomas, W.; Nicholas, E. Friction stir welding for the transportation industries. Materials & Design 1997, 18, 269-273.
8. Fuse, K.; Badheka, V. Bobbin tool friction stir welding: A review. Science and Technology of Welding and Joining 2019, 24, 277-304.
9. Wang, G.-Q.; Zhao, Y.-H.; Tang, Y.-Y. Research progress of bobbin tool friction stir welding of aluminum alloys: A review. Acta Metallurgica Sinica (English Letters), 1-17.
10. Tamadon, A.; Pons, D.J.; Clucas, D.; Sued, K. Internal material flow layers in AA6082-T6 butt-joints during bobbin friction stir welding. Metals 2019, 9, 1059.
11. Tamadon, A.; Pons, D.; Sued, K.; Clucas, D. Thermomechanical grain refinement in AA6082-T6 thin plates under bobbin friction stir welding. Metals 2018, 8, 375.
12. Tamadon, A.; Pons, D.J.; Clucas, D.; Sued, K. Texture evolution in aa6082-t6 BFSW welds: Optical microscopy and ebsd characterisation. Materials 2019, 12, 3215.
13. Sued, M.; Tamadon, A.; Pons, D. Material flow visualization in bobbin friction stir welding by analogue model. Proceedings of Mechanical Engineering Research Day 2017, 2017, 1-2.
14. Tamadon, A.; Pons, D.; Sued, K.; Clucas, D. Development of metallographic etchants for the microstructure evolution of AA6082-T6 BFSW welds. Metals 2017, 7, 423.
15. Tamadon, A.; Pons, D.; Sued, K.; Clucas, D. Formation mechanisms for entry and exit defects in bobbin friction stir welding. Metals 2018, 8, 33.
16. Sued, M.K. Fixed bobbin friction stir welding of marine grade aluminium. Ph.D. Thesis, University of Canterbury, Christchurch, New Zealand, 2015.
17. Thomas, W.; Wiesner, C.; Marks, D.; Staines, D. Conventional and bobbin friction stir welding of 12% chromium alloy steel using composite refractory tool materials. Science and Technology of Welding and Joining 2009, 14, 247-253.
18. Cui, L.; Yang, X.; Zhou, G.; Xu, X.; Shen, Z. Characteristics of defects and tensile behaviors on friction stir welded AA6061-T4 T-joints. Materials Science and Engineering: A 2012, 543, 58-68.
19. Pal, S.; Phaniraj, M.P. Determination of heat partition between tool and workpiece during FSW of SS 304 using 3D CFD modeling. Journal of Materials Processing Technology 2015, 222, 280-286.
20. Hilgert, J.; Dos Santos, J.; Huber, N. Shear layer modelling for bobbin tool friction stir welding. Science and Technology of Welding and Joining 2012, 17, 454-459.
21. Hilgert, J.; Schmidt, H.; Dos Santos, J.; Huber, N. Thermal models for bobbin tool friction stir welding. Journal of Materials Processing Technology 2011, 211, 197-204.
22. Tamadon, A.; Pons, D.; Sued, M.; Clucas, D.; Wong, E. In Analogue modelling of bobbin tool friction stir welding, Proceedings of the International Conference on Innovative Design and Manufacturing (ICIDM2016), Auckland, New Zealand, 24-26 January 2016, 2016; Auckland, New Zealand.
23. Tamadon, A.; Pons, D.; Sued, M.; Clucas, D.; Wong, E. In Preparation of plasticine material for analogue modelling, Proceedings of the International Conference on Innovative Design and Manufacturing (ICIDM2016), Auckland, New Zealand, 24-26 January 2016, 2016; Auckland, New Zealand.

24. Colligan, K. Material flow behavior during friction welding of aluminum. Welding Journal 1999, 75, 229-237.

25. Fonda, R.; Reynolds, A.; Feng, C.; Knipling, K.; Rowenhorst, D. Material flow in friction stir welds. Metallurgical and Materials Transactions A 2013, 44, 337-344.

26. Hilgert, J.; Hütsch, L.L.; dos Santos, J.; Huber, N. In Material flow around a bobbin tool for friction stir welding, Excerpt from the Proceedings of the COMSOL Conference, 2010.

27. Liechty, B.; Webb, B. Modeling the frictional boundary condition in friction stir welding. International Journal of Machine Tools and Manufacture 2008, 48, 1474-1485.

28. He, X.; Gu, F.; Ball, A. A review of numerical analysis of friction stir welding. Progress in Materials Science 2014, 65, 1-66.

29. Trueba, L.; Torres, M.A.; Johannes, L.B.; Rybicki, D. Process optimization in the self-reacting friction stir welding of aluminum 6061-T6. International Journal of Material Forming 2018, 11, 559-570.

30. Shrivastava, A.; Pfefferkorn, F.E.; Duffie, N.A.; Ferrier, N.J.; Smith, C.B.; Malukhin, K.; Zinn, M. Physics-based process model approach for detecting discontinuity during friction stir welding. The International Journal of Advanced Manufacturing Technology 2015, 79, 605-614.

31. Argesi, F.B.; Shamsipur, A.; Mirsalehi, S.E. Dissimilar joining of pure copper to aluminum alloy via friction stir welding. Acta Metallurgica Sinica (English Letters) 2018, 31, 1183-1196.

32. Wahid, M.A.; Siddiquee, A.N.; Khan, Z.A.; Asjad, M. Friction stir welds of al alloy-cu: An investigation on effect of plunge depth. Archive of Mechanical Engineering 2016, 63, 619-634.

33. Moradi, M.M.; Aval, H.J.; Jamaati, R. Effect of tool pin geometry and weld pass number on microstructural, natural aging and mechanical behaviour of sic-incorporated dissimilar friction-stir-welded aluminium alloys. Sādhanā 2019, 44, 9.

34. Gharavi, F.; Ebrahimzadeh, I.; Amini, K.; Sadeghi, B.; Dariya, P. Effect of welding heat input on the microstructure and mechanical properties of dissimilar friction stir-welded copper/brass lap joint. Materials Research 2019, 22.

35. Ting, P.L.; Tsai, C.Y.; Chiu, L.H.; Cheng, C.P. In Tensile strength and metallurgical analysis in anodized al/cu joint using friction stir welding, Key Engineering Materials, 2015; Trans Tech Publ: pp 490-495.

36. Tamadon, A.; Pons, D.J.; Clucas, D. AFM characterization of stir-induced micro-flow features within the AA6082-t6 BFSW welds. Technologies 2019, 7, 80.

37. Barcellona, A.; Buffa, G.; Fratini, L.; Palmeri, D. On microstructural phenomena occurring in friction stir welding of aluminium alloys. Journal of Materials Processing Technology 2006, 177, 340-343.

38. Fonda, R.; Bingert, J. Texture variations in an aluminum friction stir weld. Scripta Materialia 2007, 57, 1052-1055.

39. Fonda, R.; Bingert, J.; Colligan, K. Development of grain structure during friction stir welding. Scripta Materialia 2004, 51, 243-248.

40. Tamadon, A.; Pons, D.J.; Clucas, D. Structural anatomy of tunnel void defect in bobbin friction stir welding, elucidated by the analogue modelling. Applied System Innovation 2020, 3, 2.

41. Garg, A.; Raturi, M.; Bhattacharya, A. Influence of additional heating in friction stir welding of dissimilar aluminum alloys with different tool pin profiles. The International Journal of Advanced Manufacturing Technology, 1-21.
42. Wiedenhoft, A.G.; Amorim, H.J.d.; Rosendo, T.d.S.; Tier, M.A.D.; Reguly, A. Effect of heat input on the mechanical behaviour of Al-Cu FSW lap joints. Materials Research 2018, 21.
43. Schneider, J.; Cobb, J.; Carpenter, J.S.; Mara, N.A. Maintaining nano-lamellar microstructure in friction stir welding (FSW) of accumulative roll bonded (arb) cu-nb nano-lamellar composites (nlc). Journal of Materials Science & Technology 2018, 34, 92-101.
44. Saeid, T.; Abdollah-Zadeh, A.; Sazgari, B. Weldability and mechanical properties of dissimilar aluminum–copper lap joints made by friction stir welding. Journal of Alloys and Compounds 2010, 490, 652-655.
45. Muthu, M.F.X.; Jayabalan, V. Tool travel speed effects on the microstructure of friction stir welded aluminum–copper joints. Journal of Materials Processing Technology 2015, 217, 105-113.
46. Shah, L.; Othman, N.; Gerlich, A. Review of research progress on aluminium–magnesium dissimilar friction stir welding. Science and Technology of Welding and Joining 2018, 23, 256-270.
47. Tamadon, A.; Baghestani, A.; Bajgholi, M.E. Influence of wc-based pin tool profile on microstructure and mechanical properties of AA1100 FSW welds. Technologies 2020, 8, 34.
48. Sharma, N.; Siddiquee, A.N.; Khan, Z.A.; Mohammed, M.T. Material stirring during FSW of Al–Cu: Effect of pin profile. Materials and Manufacturing Processes 2018, 33, 786-794.
49. Carlone, P.; Astarita, A.; Palazzo, G.S.; Paradiso, V.; Squillace, A. Microstructural aspects in Al–Cu dissimilar joining by FSW. The International Journal of Advanced Manufacturing Technology 2015, 79, 1109-1116.
50. Xue, P.; Xiao, B.; Ni, D.; Ma, Z. Enhanced mechanical properties of friction stir welded dissimilar Al–Cu joint by intermetallic compounds. Materials Science and Engineering: A 2010, 527, 5723-5727.
51. Tamadon, A.; Pons, D.J.; Clucas, D. Microstructural study on thermomechanical behaviour of 6082-T6 aluminium BFSW weld plates. In Materials@UC 2018, Christchurch, New Zealand, 2018.
52. Tamadon, A.; Pons, D.J.; Clucas, D. Thermomechanical performance of bobbin tool design as an innovative variant for friction stir welding. In Manufacturing and Design Conference (MaD 2019) Auckland, New Zealand, 2019.
53. Tamadon, A. Characterization of flow-based bobbin friction stir welding process. Ph.D. Thesis, University of Canterbury, Christchurch, New Zealand, 2019.
54. Tamadon, A.; Pons, D.; Clucas, D. Analogue modelling of flow patterns in bobbin friction stir welding by the dark-field/bright-field illumination method. Advances in Materials Science 2020, 20, 56-70.
55. Tamadon, A.; Pons, D.J.; Clucas, D. Flow-based anatomy of bobbin friction-stirred weld; AA6082-T6 aluminium plate and analogue plasticine model. Applied Mechanics 2020, 1, 3-19.

56. Silva, B.H.; Zepon, G.; Bolfarini, C.; dos Santos, J.F. Refill friction stir spot welding of aa6082-t6 alloy: Hook defect formation and its influence on the mechanical properties and fracture behavior. Materials Science and Engineering: A 2020, 773, 138724.